Article

Toward Identification of the Compound I Reactive Intermediate in Cytochrome P450 Chemistry: A QM/MM Study of Its EPR and Mössbauer Parameters

Jan C. Schneboom, Frank Neese, and Walter Thiel

J. Am. Chem. Soc., **2005**, 127 (16), 5840-5853• DOI: 10.1021/ja0424732 • Publication Date (Web): 02 April 2005

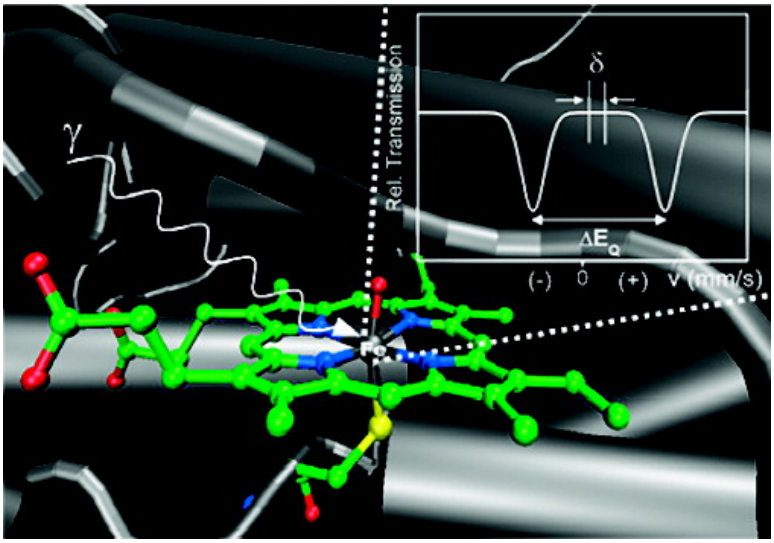

More About This Article

Additional resources and features associated with this article are available within the HTML version:

- Supporting Information
- Links to the 49 articles that cite this article, as of the time of this article download
- Access to high resolution figures
- Links to articles and content related to this article
- Copyright permission to reproduce figures and/or text from this article

View the Full Text HTML

J|A|C|S
ARTICLES
Published on Web 04/02/2005

Toward Identification of the Compound I Reactive Intermediate in Cytochrome P450 Chemistry: A QM/MM Study of Its EPR and Mössbauer Parameters

Jan C. Schöneboom,[†] Frank Neese,*[,‡] and Walter Thiel*[,†]

Contribution from the Max-Planck-Institut für Kohlenforschung, Kaiser-Wilhelm-Platz 1, D-45470 Mülheim an der Ruhr, Germany, and Max-Planck-Institut für Bioanorganische Chemie, Stiftstrasse 34-36, D-45413 Mülheim an der Ruhr, Germany

Received December 15, 2004; E-mail: neese@mpi-muelheim.mpg.de; thiel@mpi-muelheim.mpg.de

Abstract: Quantum mechanical/molecular mechanical (QM/MM) methods have been used in conjunction with density functional theory (DFT) and correlated ab initio methods to predict the electron paramagnetic resonance (EPR) and Mössbauer (MB) properties of Compound I in $P450_{cam}$. For calibration purposes, a small Fe(IV)−oxo complex $[Fe(O)(NH_3)_4(H_2O)]^{2+}$ was studied. The $^3A_2$ and $^5A_1$ states (in C_{4v} symmetry) are found to be within 0.1−0.2 eV. The large zero-field splitting (ZFS) of the $(FeO)^{2+}$ unit in the $^3A_2$ state arises from spin−orbit coupling with the low-lying quintet and singlet states. The intrinsic *g*-anisotropy is very small. The spectroscopic properties of the model complex $[Fe(O)(TMC)(CH_3CN)]^{2+}$ (TMC = 1,4,8,-11-tetramethyl-1,4,8,11-tetraazacyclotetradecane) are well reproduced by theory. In the model complexes $[Fe(O)(TMP)(X)]^+$ (TMP = tetramesitylporphyrin, X = nothing or H_2O) the computations again account for the observed spectroscopic properties and predict that the coupling of the $^5A_1$ state of the $(FeO)^{2+}$ unit to the porphyrin radical leads to a low-lying sextet/quartet manifold ∼12 kcal/mol above the quartet ground state. The calculations on cytochrome $P450_{cam}$, with and without the simulation of the protein environment by point charges, predict a small antiferromagnetic coupling ($J \approx -13$ to -16 cm^{-1}; $\hat{H}_{HDvV} = -2J\vec{S}_A\vec{S}_B$) and a large ZFS > 15 cm^{-1} (with $E/D \approx 1/3$) which will compete with the exchange coupling. This leads to three Kramers doublets of mixed multiplicity which are all populated at room temperature and may therefore contribute to the observed reactivity. The MB and ligand hyperfine couplings (^{14}N, ^1H) are fairly sensitive to the protein environment which controls the spin density distribution between the porphyrin ring and the axial cysteinate ligand.

1. Introduction

Cytochrome P450 enzymes are a family of ubiquitous metabolizing heme proteins that perform a variety of functions including biosynthesis of, for example, steroid hormones, as well as detoxification of xenobiotics.[1] The remarkable capability of P450 enzymes to catalyze oxidations, such as C−H hydroxylation or C=C epoxidation, with potentially high regio- and stereoselectivity, has generated considerable interest in clarifying the details of the mechanisms involved.[2] At least for C−H hydroxylation, the active oxidant is generally assumed to be Compound I (**1**),[3] an oxoiron(IV) porphyrin radical cation (see Scheme 1). However, while the intermediacy of its precursor in $P450_{cam}$-mediated hydroxylation, a hydroperoxy complex (see Scheme 1), has recently been ascertained spectroscopically under turnover conditions,[4] there is still no definitive experimental evidence for Compound I, and the mechanism of hydroxylation remains controversial.[5,6]

The experimental characterization of this putative species for P450 proved to be difficult due to the fast reaction steps occurring after O_2 binding. Cryogenic X-ray diffraction,[7] as well as low-temperature-trapping spectroscopic techniques[4,8] on the bacterial enzyme cytochrome $P450_{cam}$ (CYP101), has provided indirect evidence, but could not unambiguously identify Compound I. The conclusion from these studies thus is that Compound I of $P450_{cam}$ does not accumulate at a detection temperature of 200 K (or even below this temperature). On the other hand, the characterization of short-lived enzymatic intermediates is still making progress by virtue of rapid developments in spectroscopic techniques.[9] Electron paramagnetic resonance (EPR), electron nuclear double resonance (ENDOR), and Mössbauer (MB) spectroscopy, particularly in

[†] Max-Planck-Institut für Kohlenforschung.
[‡] Max-Planck-Institut für Bioanorganische Chemie.

(1) Ortiz de Montellano, P. R. Ed., *Cytochrome P450: Structure, Mechanisms and Biochemistry*, 2nd ed.; Plenum Press: New York, 1995; Vol. 2.
(2) Ortiz de Montellano, P. R.; De Voss, J. J. *Nat. Prod. Rep.* **2002**, *19*, 1.
(3) Groves, J. T.; Watanabe, Y. *J. Am. Chem. Soc.* **1988**, *110*, 8443.
(4) Davydov, R.; Makris, T. M.; Kofman, V.; Werst, D. E.; Sligar, S. G.; Hoffman, B. M. *J. Am. Chem. Soc.* **2001**, *123*, 1403.
(5) (a) Shaik, S.; de Visser, S. P.; Ogliaro, F.; Schwarz, H.; Schröder, D. *Curr. Opin. Chem. Biol.* **2002**, *6*, 556. (b) Shaik, S.; Cohen, S.; de Visser, S. P.; Sharma, P. K.; Kumar, D.; Kozuch, S.; Ogliaro, F.; Davinovich, D. *Eur. J. Inorg. Chem.* **2004**, 207.
(6) Newcomb, M.; Hollenberg, P. F.; Coon, M. J. *Arch. Biochem. Biophys.* **2003**, *409*, 72.
(7) Schlichting, I.; Berendzen, J.; Chu, K.; Stock, A. M.; Maves, S. A.; Benson, D. A.; Sweet, R. M.; Ringe, D.; Petsko, G. A.; Sligar, S. G. *Science* **2000**, *287*, 1615.
(8) Denisov, I. G.; Makris, T. M.; Sligar, S. G. *J. Biol. Chem.* **2001**, *276*, 11648.
(9) (a) Meunier, B.; de Visser, S. P.; Shaik, S. *Chem. Rev.* **2004**, *104*, 3947. (b) Slep, L. D.; Neese, F. *Angew. Chem., Int. Ed.* **2003**, *42*, 2942. (c) Trautwein, A. X.; Bill, E.; Bominaar, E. L.; Winkler, H. *Struct. Bonding* **1991**, *78*, 1.

10.1021/ja0424732 CCC: $30.25

Scheme 1

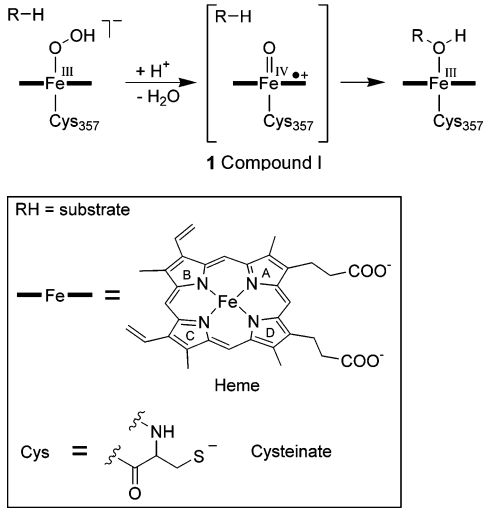

combination with rapid freeze quench techniques, are most successful in this regard and will most likely be the key techniques in future studies. For example, it was EPR, ^{1}H-, and ^{14}N-ENDOR studies on P450$_{cam}$ that have recently identified the ferric peroxy anion and the ferric hydroperoxy intermediate of this enzyme.[4] If the ongoing efforts to detect Compound I should succeed, an interpretation of the experimental spectra may be difficult (e.g., due to the presence of impurities or simply because of the complexity of the spectra). The analysis of experimental data can be significantly facilitated by theoretical predictions for the corresponding spectroscopic parameters.[10,11] The purpose of the present article is the calculation of such parameters to assist experimentalists in the ultimate detection of this species.

In this study, we focus on the prediction of exchange coupling constants, hyperfine coupling (HFC) and nuclear quadrupole coupling (NQC) tensors, the ^{57}Fe MB isomer shift, the zero-field splitting (ZFS), as well as *g*-values for Compound I of P450$_{cam}$. Because we aim at realistic predictions for the species in the enzyme environment where, for example, long-range electrostatic effects are important, we have chosen a hybrid quantum mechanical/molecular mechanical (QM/MM) approach[12] to model the full enzyme in a solvent environment. In QM/MM calculations, a confined region that is crucial for the chemical and spectroscopic properties of a system is treated at a high level of theory (by quantum mechanics, QM), while the environment is taken into account explicitly by a classical force field (molecular mechanics, MM). By treating the entire system with this combined approach, accurate predictions of the active site geometric and electronic structure are possible, while realistically accounting for the influence of the environment on the computed properties at a manageable cost. We also compare the results obtained from calculations including the enzyme environment with those of pure quantum mechanical calculations for the isolated Compound I complex in the gas phase. In doing so, we can assess the influence of the protein environment on the calculated values.

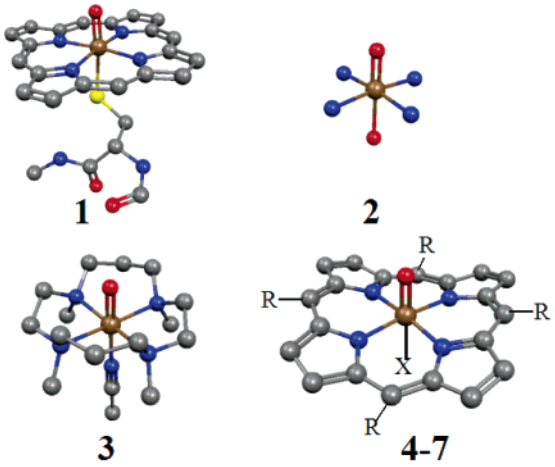

Figure 1. Structures of model systems studied in this work. **1** = Compound I, **2** = $[Fe(O)(NH_3)_4(H_2O)]^{2+}$, **3** = $[Fe(O)(TMC)(CH_3CN)]^{2+}$, **4**−**7** = $[Fe(O)(P)(X)]^{+}$ (**4**: X = nothing, R = C_6H_5; **5**: X = H_2O, R = C_6H_5; **6**: X = nothing, R = H; **7**: X = H_2O, R = H). Hydrogen atoms are omitted for clarity.

The accurate prediction of EPR and MB data of transition metal complexes by quantum mechanical calculations is a challenge to contemporary computational chemistry.[10,11] Consequently, it is necessary to test the accuracy of our approach by comparison to available experimental data. To this end, we have carried out density functional theory (DFT) and ab initio calculations on (i) a recently reported non-heme oxoferryl complex $[Fe(TMC)(O)(CH_3CN)]^{2+}$, TMC = 1,4,8,11-tetramethyl-1,4,8,11-tetraazacyclotetradecane,[13] and (ii) oxoferryl porphyrin π cation radical complexes as models for native Compound I, that is, tetramesitylporphyrin (TMP) and tetrakis-(2,6-dichlorophenyl)porphyrin (TDCPP) derivatives, where results from EPR and MB studies are available.[14] The model systems investigated presently are shown in Figure 1.

There are many previous computational studies on Compound I species that have most recently been comprehensively reviewed.[15] Most relevant to the present work are previous QM/MM studies of Compound I[16−18] as well as DFT calculations of gas-phase models that address the electronic structure and properties of Compound I species,[19−21] in particular hyperfine coupling constants as well as MB parameters.[22,23] On the

(10) Neese, F. *Curr. Opin. Chem. Biol.* **2003**, *7*, 125.
(11) Neese, F.; Solomon, E. I. In *Magnetoscience: From Molecules to Materials*; Miller, J. S., Drillon, M., Eds.; Wiley: New York, 2002; Vol. 4, p 345.
(12) (a) Warshel, A.; Levitt, M. *J. Mol. Biol.* **1976**, *103*, 227. (b) Field, M. J.; Bash, P. A.; Karplus, M. *J. Comput. Chem.* **1990**, *11*, 700. (c) Gao, J. In *Reviews in Computational Chemistry*; Lipkowitz, K. B., Boyd, D. B., Eds.; VCH: New York, 1996; Vol. 7, p 119. (d) Mordasini, T. Z.; Thiel, W. *Chimia* **1998**, *58*, 288. (e) Monard, G.; Merz, K. M. *Acc. Chem. Res.* **1999**, *32*, 904.
(13) Rohde, J.-U.; In, J.-H.; Lim, M. H.; Brennessel, W. W.; Bukowski, M. R.; Stubna, A.; Münck, E.; Nam, W.; Que, L., Jr. *Science* **2003**, *299*, 1037.
(14) Mandon, D.; Weiss, R.; Jayaraj, K.; Gold, A.; Terner, J.; Bill, E.; Trautwein, A. X. *Inorg. Chem.* **1992**, *31*, 4404.
(15) Shaik, S.; Kumar, D.; de Visser, S. P.; Altun, A.; Thiel, W. *Chem. Rev.*, published online March 17, 2005, http://dx.doi.org/10.1021/cr030722j.
(16) Schöneboom, J. C.; Lin, H.; Reuter, N.; Thiel, W.; Cohen, S.; Ogliaro, F.; Shaik, S. *J. Am. Chem. Soc.* **2002**, *124*, 8142.
(17) Schöneboom, J. C.; Cohen, S.; Lin, H.; Shaik, S.; Thiel, W. *J. Am. Chem. Soc.* **2004**, *126*, 4017.
(18) (a) Guallar, V.; Friesner, R. A. *J. Am. Chem. Soc.* **2004**, *126*, 8051 (b) Guallar, V.; Baik, M.; Lippard, S. J.; Friesner, R. A. *Proc. Natl. Acad. Sci. U.S.A.* **2003**, *100*, 6998.
(19) (a) Loew, G. H.; Harris, D. L. *Chem. Rev.* **2000**, *100*, 407. (b) Loew, G. H. *Int. J. Quantum Chem.* **2000**, *77*, 54. (c) Rydberg, P.; Sigfridsson, E.; Ryde, U. *J. Biol. Inorg. Chem.* **2004**, *9*, 203. (d) Antony, J.; Grodzicki, M.; Trautwein, A. X. *J. Phys. Chem. A* **1997**, *101*, 2692.
(20) (a) Green, M. T. *J. Am. Chem. Soc.* **2001**, *123*, 9218. (b) Green M. T. *J. Am. Chem. Soc.* **1999**, *121*, 7939.
(21) (a) Green, M. T.; Dawson, J. H.; Gray, H. B. *Science* **2004**, *304*, 1653 (b) Green, M. T. *J. Am. Chem. Soc.* **1998**, *120*, 10772
(22) Zhang, Y.; Oldfield, E. *J. Am. Chem. Soc.* **2004**, *126*, 4470.
(23) Kuramochi, H.; Noodleman, L.; Case, D. A. *J. Am. Chem. Soc.* **1997**, *119*, 11442.

experimental side, Que and co-workers were the first to structurally characterize the $(FeO)^{2+}$ motif in non-heme iron systems.[13,24] Decker et al. reported absorption and magnetic circular dichroism (MCD) spectra of such a non-heme complex, made spectral assignments, and discussed the electronic structure of the Fe═O bond based on DFT calculations.[25]

The present article is the first comprehensive theoretical study on spin Hamiltonian parameters for Compound I of P450 enzymes, presenting results from density functional theory and correlated ab initio calculations. To the best of our knowledge, it is also the first time that QM/MM calculations have been used to calculate EPR and MB data of a metalloenzyme. The article is organized as follows. We first calibrate the theoretical methodology on the smallest reasonable model of a prototype $(FeO)^{2+}$ core (**2**) where high-level ab initio calculations are still feasible. The calculations on the recently reported complex **3** allow for comparison with experimental data. The extensions to models **4**−**7** address the influence of a porphyrin radical on the properties of the $(FeO)^{2+}$ unit. Finally, the calculations are extended to the Compound I model **1** in Figure 1, which is investigated both with external point charges simulating the electrostatic field of the surrounding protein and without these interactions.

2. Computational Details

A. Ab Initio Calculations. The ab initio calculations employed the iron basis set devised by Wachters[26] (14s11p6d3f contracted as {62111111/332111/3111/21}) and the aug-cc-pVDZ basis set[27] on the oxo group (18s5p2d contracted as {8811/311/11}). In the small $(FeO)^{2+}$ model $[FeO(NH_3)_4(H_2O)]^+$ (**2**) the ligands were described by the SV(P) basis set.[28] For the larger porphyrin models **6** and **7** the polarization functions on the ligands had to be deleted. However, in the Compound I models **1** and **4**−**7** the directly coordinating nitrogen atoms and the sulfur ligand could still be described with the larger and more accurate TZVP basis.[29] Ab initio calculations of excitation energies were carried out with the spectroscopy oriented configuration interaction (SORCI) method.[30] These calculations were done with the thresholds $T_{sel} = 10^{-6}$ E_h, $T_{pre} = 10^{-5}$, and $T_{nat} = 10^{-5}$ at which stage excitation energies are converged within ∼0.1 eV of the SORCI limit.[31] Details of the difference dedicated configuration interaction (DDCI) implementation used in the present study can be found in ref 30. The input orbitals for the SORCI calculations were spin-restricted DFT orbitals generated with the BP86 functional. Experience indicates that the precise form of the functional is not of importance but that DFT orbitals are usually more suitable than Hartree−Fock orbitals for starting correlated calculations on transition metal complexes.[32,33]

B. DFT and DFT/MM Calculations. Unless noted otherwise, all DFT calculations employed the B3LYP density functional. This hybrid functional often gives better results for transition metal compounds than pure gradient-corrected functionals, especially with regard to metal−ligand covalency.[11]

DFT Calculations on 4 and 5. Geometry optimizations were carried out without symmetry constraints and employed the SV(P) basis set.[28] The quartet and the doublet spin state were separately optimized with tight convergence criteria. In agreement with the experimental assignment,[14] we found the quartet state to be the ground state, being more stable than the doublet by ca. 0.1 kcal/mol (see discussion in sections 3C and 3D). The hyperfine tensor and the MB properties were obtained from subsequent single-point calculations with the triply polarized CP(PPP) basis set[34] on iron. In these calculations, the other atoms were assigned the SV(P) basis set;[28] however, the inner s-functions were left completely uncontracted. For the iron atom, an enhanced integration grid was used, and the overall integration accuracy was increased to 7.0 as explained in ref 34. The **g**-tensors as well as the exchange coupling constants were computed with the TZVP basis[29] at all atoms.

DFT (Gas Phase) and DFT/MM Calculations on Compound I (1). Optimized geometries of Compound I in the gas phase as well as in the protein environment were taken from a previously published QM/MM study[16] on Compound I of cytochrome $P450_{cam}$. QM/MM optimizations were carried out separately for the doublet and quartet states. The isolated QM regions (^{2}A and ^{4}A state) were then reoptimized in the gas phase at the B3LYP level with the same basis set. The former calculations will be abbreviated as S_p (system in the protein environment) and the latter as S_g (system in the gas phase). In the QM/MM calculations, an electronic embedding scheme[35] was used, that is, the fixed MM charges (CHARMM22) were included into the one-electron Hamiltonian of the QM calculation and the QM/MM electrostatic interactions were evaluated from the QM electrostatic potential and the MM atomic charges. No cutoffs were introduced for the nonbonding MM and QM/MM interactions. Spectroscopic parameters of the species in the protein (gas phase) were obtained from single-point calculations at the B3LYP/CHARMM22 (B3LYP) level, with the same basis sets described above for the model compounds (i.e., iron CP(PPP) and decontracted SV(P) basis set in the MB and HFC calculations; TZVP basis for *g*-value and *J* parameter computations). The calculated hyperfine- and **g**-tensors of the broken-symmetry (BS) doublet state were corrected by spin projection as described in the Supporting Information.[36]

C. Calculation of Spectroscopic Parameters. The calculation of the various MB and EPR spectroscopic parameters is associated with a substantial number of technical details, which are summarized in the Supporting Information.

D. Programs. All spectroscopic parameters were calculated with the ORCA 2.2.74 and ORCA 2.4.10 program packages.[37] The ab initio electronic structure calculations were carried out with the multireference configuration interaction (MR-CI) module of ORCA. For the DFT treatment in the DFT/MM as well as in the pure DFT geometry optimizations, we employed the TURBOMOLE program.[38] For the QM/MM coupling, we used the ChemShell package.[39] The force field parameters for the MM part were taken from CHARMM22.[40,41] Coupled cluster calculations were done with the *Gaussian03* pogram.[42]

(24) Costas, M.; Mehn, M. P.; Jenser, M. P.; Que, L., Jr. *Chem. Rev.* **2004**, *104*, 939.
(25) Decker, A.; Rohde, J.-U.; Que, L., Jr.; Solomon, E. I. *J. Am. Chem. Soc.* **2004**, *126*, 5378.
(26) (a) Wachters, A. J. H. *J. Chem. Phys.* **1970**, *52*, 1033. (b) Hay, P. J. *J. Chem. Phys.* **1977**, *66*, 4377. (c) Bauschlicher, C. W.; Langhoff, S. R.; Barnes, L. A. *J. Chem. Phys.* **1989**, *91*, 2399.
(27) Dunning, T. H., Jr. *J. Chem. Phys.* **1989**, *90*, 1007.
(28) Schäfer, A.; Horn, H.; Ahlrichs, R. *J. Chem. Phys.* **1992**, *97*, 2571.
(29) Schäfer, A.; Huber, C.; Ahlrichs, R. *J. Chem. Phys.* **1994**, *100*, 5829.
(30) Neese, F. *J. Chem. Phys.* **2003**, *119*, 9428.
(31) Wanko, M.; Hoffmann, M.; Strodel, P.; Koslowski, A.; Thiel, W.; Neese, F.; Frauenheim, T.; Elstner, M. *J. Phys. Chem. B* **2005**, *109*, 3606.
(32) Hupp, T.; Engels, B.; Della Sala, F.; Görling, A. *Chem. Phys. Lett.* **2002**, *360*, 175.
(33) Neese, F. *Magn. Reson. Chem.* **2004**, *42*, S187.
(34) Neese, F. *Inorg. Chim. Acta* **2002**, *337*, 181.
(35) Bakowies, D.; Thiel, W. *J. Phys. Chem.* **1996**, *100*, 10580.
(36) In contrast to the spin density, the electron density of the antiferromagnetic state is well described by the broken symmetry formalism; thus no spin projection had to be applied in the calculation of the Mössbauer parameters.
(37) Neese, F. *ORCA*, version 2.4, revision 10; Max-Planck Institut für Bioanorganische Chemie: Mülheim a. d. Ruhr, Germany, 2004.
(38) (a) Ahlrichs, R.; Bär, M.; Häser, M.; Horn, H.; Kölmel, C. *Chem. Phys. Lett.* **1989**, *162*, 165. (b) Ahlrichs, R.; Bär, M.; Baron, H.-P.; Bauernschmitt, R.; Böcker, S.; Ehrig, M.; Eichkorn, K.; Elliot, S.; Furche, F.; Häser, M.; Horn, H.; Hättig, C.; Huber, C.; Huniar, U.; Kattanneck, M.; Köhn, A.; Kölmel, C.; Kollwitz, M.; May, K.; Ochsenfeld, C.; Öhm, H.; Schäfer, A.; Schneider, U.; Treutler, O.; v. Arnim, M.; Weigend, F.; Weis, P.; Weiss, H. *TURBOMOLE*, 5.5; University of Karlsruhe: Karlsruhe, Germany, 2002.
(39) Sherwood, P.; de Vries, A. H.; Guest, M. F.; Schreckenbach, G.; Catlow, C. R. A.; French, S. A.; Sokol, A. A.; Bromley, S. T.; Thiel, W.; Turner, A. J.; Billeter, S.; Terstegen, F.; Thiel, S.; Kendrick, J.; Rogers, S. C.; Casci, J.; Watson, M.; King, F.; Karlsen, E.; Sjovoll, M.; Fahmi, A.; Schäfer, A.; Lennartz, C. *J. Mol. Struct. (THEOCHEM)* **2003**, *632*, 1.

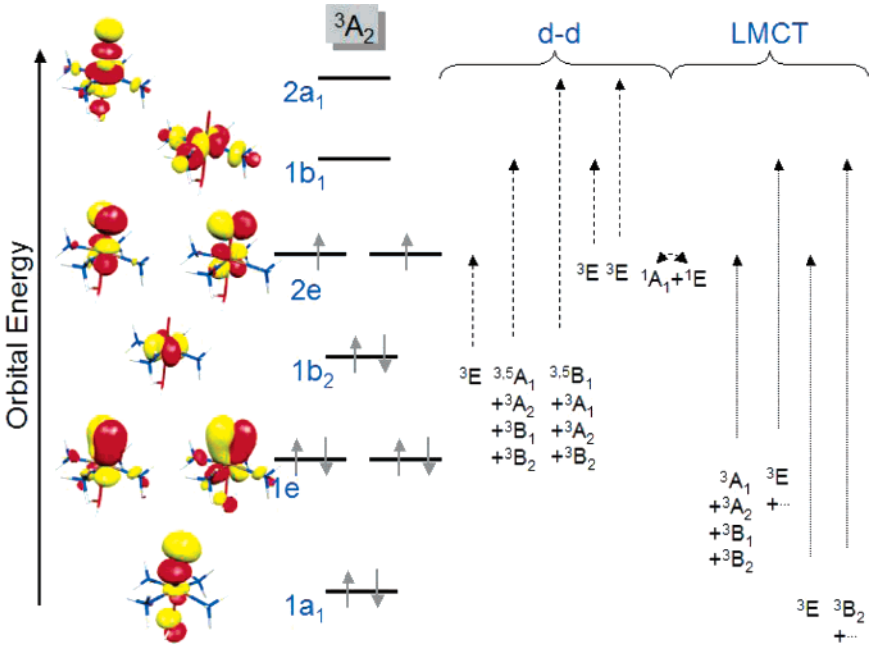

Figure 2. The most important orbitals (from B3LYP DFT calculations) of the $(FeO)^{2+}$ motif in the upper valence region (analyzed under approximate C_{4v} symmetry) and term symbols arising from elementary single excitations. The indicated orbital occupation pattern refers to the $^3A_2$ ground state.

3. Results

A. Study on $[Fe(O)(NH_3)_4(H_2O)]^{2+}$ (2). Electronic Structure. The initial study on model **2** ($[Fe(O)(NH_3)_4(H_2O)]^{2+}$) focused on the term scheme of the FeO unit and the contributions of the various excited states to the spectroscopic parameters. These calculations serve a dual purpose: (a) it is important to understand the origin of the local contributions to the observable properties of the spin-coupled system which may to a reasonable approximation be constructed using vector coupling procedures[43,44] and (b) the ab initio results serve to calibrate the DFT methods used for the larger systems. We have deliberately not employed a thiolate ligand in order to keep the analysis simple since the thiolate ligand, due to its very soft character, significantly adds to the complexity of the electronic structure.

The orbital structure of the FeO unit (see Figure 2) is well-known and follows the general expectations for metal−oxo complexes.[22,23,45,46] The possible ground-state multiplicities in the low-symmetry split d^4 configuration are $S = 0$, $S = 1$, or $S = 2$. The majority of $(FeO)^{2+}$ complexes show a $S = 1$ ground state even though $S = 2$ has been observed in a model complex[47] and more recently also as a reaction intermediate in the catalytic cycle of the TauD enzyme.[48] Here we focus on the $S = 1$ manifold since this is the relevant local spin for Compound I and also the dominant spin state observed in model complexes.[24] In this spin state, six electrons occupy three orbitals that describe a strong Fe−O σ-bond and two Fe−O π-bonds. The primarily metal-centered orbitals in the distorted octahedral environment are made up of three t_{2g}-derived orbitals and two e_g-derived orbitals. The t_{2g}-set is strongly split by the interaction of the central iron with the oxo group into an essentially nonbonding, doubly occupied $1b_2(d_{xy})$-based orbital (in approximate C_{4v} symmetry) and the two $2e(d_{xz,yz})$-based orbitals, which are strongly π-antibonding with the oxo $p_{x,y}$ orbitals and which are both singly occupied. The $1b_2(d_{xy})/2e(d_{xz,yz})$ splitting is usually in the range of 1−2 eV in other metal oxo complexes.[45,46] The e_g-based orbitals are made up of the lower energy $1b_1(d_{x^2-y^2})$-based orbital which is σ-antibonding with the equatorial ligands while the higher-lying $2a_1(d_{z^2})$-based orbital is strongly σ-antibonding with the oxo group.

(40) CHARMM22 force field: MacKerell, A. D., Jr.; Bashford, D.; Bellott, M.; Dunbrack, R. L., Jr.; Evanseck, J. D.; Field, M. J.; Fischer, S.; Gao, J.; Guo, H.; Ha, S.; Joseph-McCarthy, D.; Kuchnir, L.; Kuczera, K.; Lau, F. T. K.; Mattos, C.; Michnick, S.; Ngo, T.; Nguyen, D. T.; Prodhom, B.; Reiher, W. E., III; Roux, B.; Schlenkrich, M.; Smith, J. C.; Stote, R.; Straub, J.; Watanabe, M.; Wiorkiewicz-Kuczera, J.; Yin, D.; Karplus, M. *J. Phys. Chem. B* **1998**, *102*, 3586.
(41) For details about the generation and geometric features of the snapshot structures, nonstandard force field parameters, and QM/MM geometry optimizations, see ref 16 and Supporting Information thereof.
(42) Frisch, M. J.; Trucks, G. W.; Schlegel, H. B.; Scuseria, G. E.; Robb, M. A.; Cheeseman, J. R.; Montgomery, J. A., Jr.; Vreven, T.; Kudin, K. N.; Burant, J. C.; Millam, J. M.; Iyengar, S. S.; Tomasi, J.; Barone, V.; Mennucci, B.; Cossi, M.; Scalmani, G.; Rega, N.; Petersson, G. A.; Nakatsuji, H.; Hada, M.; Ehara, M.; Toyota, K.; Fukuda, R.; Hasegawa, J.; Ishida, M.; Nakajima, T.; Honda, Y.; Kitao, O.; Nakai, H.; Klene, M.; Li, X.; Knox, J. E.; Hratchian, H. P.; Cross, J. B.; Adamo, C.; Jaramillo, J.; Gomperts, R.; Stratmann, R. E.; Yazyev, O.; Austin, A. J.; Cammi, R.; Pomelli, C.; Ochterski, J. W.; Ayala, P. Y.; Morokuma, K.; Voth, G. A.; Salvador, P.; Dannenberg, J. J.; Zakrzewski, V. G.; Dapprich, S.; Daniels, A. D.; Strain, M. C.; Farkas, O.; Malick, D. K.; Rabuck, A. D.; Raghavachari, K.; Foresman, J. B.; Ortiz, J. V.; Cui, Q.; Baboul, A. G.; Clifford, S.; Cioslowski, J.; Stefanov, B. B.; Liu, G.; Liashenko, A.; Piskorz, P.; Komaromi, I.; Martin, R. L.; Fox, D. J.; Keith, T.; Al-Laham, M. A.; Peng, C. Y.; Nanayakkara, A.; Challacombe, M.; Gill, P. M. W.; Johnson, B.; Chen, W.; Wong, M. W.; Gonzalez, C.; Pople, J. A. *Gaussian 03*, revision B.05; Gaussian, Inc.: Pittsburgh, PA, 2003.
(43) Bencini, A.; Gatteschi, D. *EPR of Exchange Coupled Systems*; Springer: Heidelberg, 1990.
(44) Slep, L. D.; Mijovilovich, A.; Meyer-Klaucke, W.; Weyhermüller, T.; Bill, E.; Bothe, E.; Neese, F.; Wieghardt, K. *J. Am. Chem. Soc.* **2003**, *125*, 15554.
(45) (a) Jørgensen, C. K. *Acta Chem. Scand.* **1957**, *11*, 73. (b) Ballhausen, C. J.; Gray, H. B. *Inorg. Chem.* **1962**, *1*, 111. (c) Paine, T.; Bothe, W.; Bill, E.; Weyhermüller, T.; Slep, L.; Neese, F.; Chaudhuri, P. *Inorg. Chem.* **2004**, *43*, 7324.
(46) (a) Harris, D. L.; Loew, G. H. *J. Am. Chem. Soc.* **1998**, *120*, 8941. (b) Neese, F.; Zaleski, J. M.; Loeb, K. E.; Solomon, E. I. *J. Am. Chem. Soc.* **2000**, *122*, 11703. (c) Lehnert, N.; Ho, R. Y. N.; Que, L., Jr.; Solomon, E. I. *J. Am. Chem. Soc.* **2001**, *123*, 8271. (d) Siegbahn, P. E. M.; Crabtree, R. H. In *Metal-Oxo and Metal-Peroxo Species in Catalytic Oxidations*; Meunier, B., Ed.; Springer: Berlin, 2000; Vol. 97, p 125. (e) Wirstam, M.; Blomberg, M. R. A.; Siegbahn, P. E. M. *J. Am. Chem. Soc.* **1999**, *121*, 10178.
(47) Kostka, K. L.; Fox, B. G.; Hendrich, M. P.; Collins, T. J.; Rickard, C. E. F.; Wright, L. J.; Münck, E. *J. Am. Chem. Soc.* **1993**, *115*, 6746.
(48) Price, J. C.; Barr, E. W.; Tirupati, B.; Bollinger, J. M.; Krebs, C. *Biochemistry* **2004**, *43*, 1134.

Table 1. Energies (in eV) of Different Spin States Relative to the $^3A_2$ State of **2** Calculated with Different Methods at the B3LYP-Optimized Geometry of the $^3A_2$ State

	$^5A_1$	^1E	$^1A_1$
SORCI(4,5)	0.06	0.70	1.07
SORCI(20,13)	−0.11	0.71	1.14
B3LYP	0.75	1.31	
UCCSD	0.02	0.80	
UCCSD(T)	0.22	0.59	

The polarity of the FeO double bond is essentially determined by the composition of the 1e(π) and 2e($d_{xz,yz}$) π*-orbitals. Furthermore, the spin density distribution is dominated by the two singly occupied 2e($d_{xz,yz}$) π*-orbitals. Thus, the higher the spin population on the central iron the more ionic the bond with the polarity $Fe^{4+}O^{2-}$, while the spin density on the oxo ligand reflects the oxo-to-iron charge donation, which is expected to be large. In the B3LYP calculations one finds spin populations of 1.15 and 0.87 (Löwdin partitioning) on the iron and oxo groups, respectively, thus showing the expected high degree of covalency. These numbers are in good agreement with the SORCI values, which are 1.11 and 0.87. We note in passing that our interpretation of the large spin density in the $(FeO)^{2+}$ system is identical with that proposed by Decker et al.[25] That is, the large spin density on the oxo ligand arises purely from covalent delocalization, as opposed to genuine Fe(III)-oxyl diradical character.[49]

Low-Lying Electronic States. The lowest triplet state has $^3A_2$ symmetry (Figure 2). The lowest quintet state is of $^5A_1$ symmetry and arises from the $1b_2(d_{xy}) \rightarrow 1b_1(d_{x^2-y^2})$ excitation. The lowest singlet states arise from singlet spin coupling in the 2e($d_{xz,yz}$) shell which yields ^1E and $^1A_1$ states in analogy to the situation found in the lowest $^1\Delta_g$ and $^1\Sigma_g^+$ states of the O_2 molecule which also arise from singlet spin coupling of two π* electrons. As long as no perturbation splits the 2e(d_{xz},d_{yz}) set, the singlets can never be the ground state due to Hund's rule. The energies of the three states relative to the $^3A_2$ ground state were calculated using the SORCI, spin-unrestricted B3LYP, and spin-unrestricted coupled cluster methods with single, double, and perturbative triple excitations (UCCSD(T)) at the B3LYP-optimized geometry for the $^3A_2$ ground state. With single reference methods (DFT, CC) the proper multiplet splitting in the singlet state is difficult to obtain, and only the lowest closed-shell solution representing a mixture of $^1A_1$ and ^1E states was computed in the present work.

The calculated splittings are collected in Table 1. The highest level multireference calculation that we are presently able to perform is the SORCI calculation with tight thresholds and a complete active space with 20 electrons in 13 orbitals (SORCI-(20,13)). The 13 MOs are the five metal d-based MOs, the three Fe═O bonding MOs, and the five metal−ligand bonding MOs which describe the σ-bonds to the equatorial ligands. The results of this calculation are expected to be balanced and show a slight preference for the $^5A_1$ state (0.11 eV below $^3A_2$, Table 1), which is, however, geometry-dependent as will be elaborated later in the article. The SORCI(4,5) treatment, which correlates the four electrons in the metal d-shell in five MOs, puts the $^5A_1$ state slightly above the $^3A_2$ state (by 0.06 eV). Both SORCI calculations give very similar results for the energies of the first excited singlet states. The B3LYP method is obviously biased in favor of the $^3A_2$ state (0.75 eV below $^5A_1$). It is well-known that relative spin state energies from hybrid DFT results are strongly (but approximately linearly) dependent on the amount of HF exchange mixed into the hybrid functional.[50] The UCCSD and UCCSD(T) calculations also show preference for the $^3A_2$ state, with results being within 0.3 eV of the largest SORCI calculation. However, it should be noted that there are some large cluster amplitudes (>0.2 in magnitude) in the UCCSD wave function, which limits the reliability of these calculations. We believe that the best estimate will probably lie between the SORCI and UCCSD(T) results, and consequently we cannot be sure whether the $^5A_1$ or $^3A_2$ state is lowest in **2**.

Since the results for **2** were obtained with a relatively small basis set, which is also applicable to larger molecules, it is important to test whether basis set incompleteness is a major source of error. We have therefore carried out additional SORCI calculations with two much larger basis sets.[51] At the SORCI-(4,5)/LARGE-I level, the triplet−quintet gap was calculated to be −0.02 eV, which is within 0.08 eV of the result in Table 1. At the even more accurate SORCI(4,5)/LARGE-II level, the triplet−quintet splitting was 0.07 eV, in almost quantitative agreement with the gap obtained with the small basis set (Table 1).[52] Thus, these results confirm that the computed relative energies are not much affected by the size of the employed basis set and that, at the SORCI level, the $^3A_2$ and $^5A_1$ states are nearly degenerate in **2**. This will also turn out to be important for the analysis of the spectroscopic parameters below. The order of such nearly degenerate states, which arise from *different* orbital configurations, is difficult to predict since all known quantum chemical methods that are applicable to molecules of this size are only accurate to ∼0.1−0.2 eV. Small variations in the geometry and electronic structure of the $(FeO)^{2+}$ unit are expected to give rise to significant changes of the relative energies of $^3A_2$ and $^5A_1$ and consequently also to significant changes in the spectroscopic parameters as will be described later in the article.

Optical Properties. Detailed SORCI calculations on the expected ligand field and LMCT transitions of **2** have been performed and are fully documented in the Supporting Information. The calculations lead to good agreement with the assignment of Decker et al. on **3**.[25]

Magnetic Properties. To interpret the **g**-tensor and the **D**-tensor of the $(FeO)^{2+}$ unit, it is important to know the selection rules of the spin−orbit coupling (SOC) operator. Under C_{4v} symmetry, the *z*-component transforms as A_2 and the *x*,*y*-components as E. Thus, the $^3A_2$ ground state has nonzero SOC

(49) Balland, W.; Charlot, M. F.; Banse, F.; Girerd, J. J.; Mattioli, T. A.; Bill, E.; Bartoli, J. F.; Battioni, P.; Mansuy, D. *Eur. J. Inorg. Chem.* **2004**, *2*, 301.

(50) Reiher, M.; Salomon, O.; Hess, B. A. *Theor. Chem. Acc.* **2001**, *107*, 48.

(51) The first calculation (LARGE-I) employed the Wachters basis on iron as before; however, the aug-TZVPP basis was applied to the oxo−oxygen and the TZVPP basis to the remaining heavy atoms. The hydrogens were described with the TZVP basis. The second calculation (LARGE-II) replaced the Wachters basis with a quadruple-ζ basis from the TurboMole library (Weigend F.; Furche, F.; Ahlrichs, R. *J. Chem. Phys.* **2003**, *119*, 12753). In addition, a second set of polarizing p-functions were added to the hydrogens. All polarization exponents were taken from the TurboMole library accessible at ftp://ftp.chemie.uni-karlsruhe.de/pub/basen (March 2005).

(52) The largest calculation that we have done was at the SORCI(20,13)/LARGE-I level with tight thresholds ($T_{Sel} = 10^{-7}\ E_h$, $T_{pre} = 10^{-5}$, and $T_{nat} = 10^{-6}$). This calculation led to up to ∼1500 reference configuration state functions (CSFs) and first-order interacting spaces of up to 4×10^{10} CSFs from which up to 9×10^6 were variationally treated. At this level, the quintet state is predicted to be 0.14 eV lower than the triplet state.

with A_1 states via the *z*-component and with E-states via the *x*- and *y*-components. The details of a qualitative model emphasizing the critical importance of the low-lying triplet, quintet, *and* singlet excited states for causing the very large ZFS characteristic of the $(FeO)^{2+}$ motif are presented in the Supporting Information. It is most important to point out that, in contrast to the ZFS tensor, the anisotropy of the **g**-tensor contains *no* contributions from the low-lying singlet and quintet states.[53]

The **g**-tensor calculated with the B3LYP method shows surprisingly small deviations from the free electron *g*-value with a small positive shift of $\Delta g_{||} = 3.7$ ppt along the Fe=O bond and a slightly larger shift of $\Delta g_{\perp} = +13.7$ ppt perpendicular to it. These results suggest that the $\Delta g_{\perp}$-value is dominated by the contributions from the $^3E(1b_2 \rightarrow 2e)$ state since this is the only one of the three d−d-based excited E-states that is expected to give rise to a positive *g*-shift since it is a transition from a doubly occupied to a singly occupied orbital.[11,53]

More relevant for the present study is the origin of the ZFS splitting tensor since its value will dominate the EPR behavior of the $S_t = {}^3/_2$ state in Compound I. Quantitative predictions of the **D**-tensor were carried out with a recently proposed quasi-restricted DFT method for the ZFS (see Supporting Information). At the BP86 level we arrive at a *D*-value of $+11.9$ cm^{-1} for **1** ($E/D = 0$). Our limited experience indicates that this methodology tends to give reliable signs and orders of magnitudes for the ZFS while somewhat underestimating its absolute values. A detailed inspection of the results shows that 6.3 cm^{-1} (53%) of the *D*-value comes from the spin-conserving excitations into and from the SOMOs and the remaining 47% from the spin-forbidden excitations. The spin singlet states contribute $+3.5$ cm^{-1}, while the quintets give $+2.1$ cm^{-1}. On the basis of the analysis of the ZFS in **3** presented in the Supporting Information, the latter value is expected to be strongly underestimated.

B. Study on the Non-Heme FeO Model Complex 3. Que and co-workers have recently succeeded in preparing and characterizing a number of high-valent Fe(IV)=O complexes.[13,24] This important contribution opens a fascinating view of the electronic structure of the Fe=O unit in the absence of coupling radicals or porphyrin ligands.[13,24] Oldfield et al. have used the model complex **3** to calibrate their DFT MB calculations against experiment.[22] To make a fair comparison to their results we have also included the complex **3** in our study and have computed its MB and EPR properties.

Geometry. The predicted structure at the BP86 level is in favorable agreement with the experimental observations (Table 2). In particular, the crucial Fe=O distance is reproduced very well in the calculations (calcd: 1.645 Å, expt: 1.646(3) Å) consistent with other DFT calculations on high-valent metal species.[46] By contrast, the average equatorial bond distances to the more weakly bonding nitrogens are overestimated by ~0.05 Å (calcd: 2.140 Å, expt: 2.090 Å), while the distance to the weakly coordinating acetonitrile molecule in the axial position is predicted well (calcd: 2.076 Å, expt: 2.057 Å). These results are very similar to the BPW91 results.[22] The B3LYP-optimized structure is similar to the BP86-optimized structure with the exception of the axial ligand distance, which is overestimated by ~0.07 Å. We note that somewhat better equatorial bond distances (average ~2.07 Å) are predicted with the local density approximation (LDA) perhaps due to a fortunate cancellation of errors that involves the well-known overbinding of the LDA method. However, the distance to the axial H_3CCN, which is well-predicted by BP86, is clearly too short in the LDA-optimized structure. The Fe=O bond is very similar in all calculations, perhaps because it is quite stiff.

Table 2. Comparison of Experimental and Optimized Bond Distances (in Å) for **3**

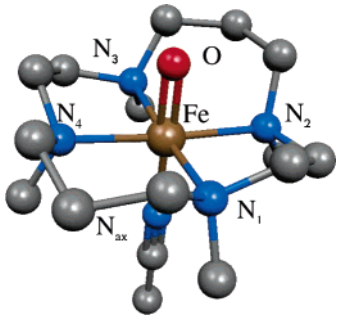

	expt[a]	BPW91[b]	BP86[c]	B3LYP[c]	LDA[c]
R(Fe=O)	1.646	1.650	1.645	1.625	1.632
R(Fe−N_{ax})	2.057	2.075	2.076	2.131	1.963
R(Fe−N_1)	2.068	2.130	2.123	2.124	2.057
R(Fe−N_2)	2.110	2.162	2.157	2.135	2.092
R(Fe−N_3)	2.116	2.162	2.155	2.157	2.091
R(Fe−N_4)	2.066	2.130	2.123	2.124	2.054

[a] Reference 13. [b] Reference 22. [c] This work.

Table 3. SORCI and B3LYP Energies (in eV) of Different Spin States Relative to the $^3A_2$ Ground State of **3**, Calculated at Various Geometries Obtained for the $^3A_2$ State

	geometry	$^5A_1$	^1E	$^1A_1$
SORCI(4,5)	BP86-opt	−0.40	0.77	0.90
	B3LYP-opt	−0.47	0.77	0.98
	LDA-opt	−0.07	0.80	0.97
	X-ray[a]	−0.12	0.78	0.96
B3LYP	BP86-opt	0.38	1.24	
	B3LYP-opt	0.38	1.25	
	LDA-opt	0.76	1.21	
	X-ray[a]	0.65	1.25	

[a] The experimental structure was obtained under code WUSJOJ from the Cambridge Structural Database.

Electronic Structure. The overall electronic structure for **3** is analogous to that obtained for the small model **2** in the previous section. The calculated Löwdin spin populations at the B3LYP level are 1.29 on Fe and 0.79 on the oxo ligand, indicating an oxo-to-iron charge donation slightly lower than that in the simplified model **2**. Again, the agreement with the SORCI values is good (1.17 on Fe and 0.82 on O).

Low-Lying Electronic States. The energies of the different spin states are expected to follow the same pattern for **2** and **3**, but there will be quantitative differences due to changes in the ligand field (Table 3). The ground state is computed to be $^5A_1$ by SORCI and $^3A_2$ by B3LYP. However, the splitting of the two states depends noticeably on the geometry. With the BP86 (or B3LYP)-optimized structure, the equatorial ligand field must be underestimated since the Fe=O bond is predicted accurately while the Fe−N bonds are predicted to be too long, thus leading to an underestimation of the σ-interaction and of the energy of the σ-antibonding $1b_1(d_{x^2-y^2})$ MO. With the LDA-optimized or X-ray structures this is not the case, and since the splitting of the $1b_2(d_{xy})$ and $1b_1(d_{x^2-y^2})$ MOs determines the position of the $^5A_1$ state relative to $^3A_2$ the SORCI calculations give a more

(53) Neese, F.; Solomon, E. I. *Inorg. Chem.* **1998**, *37*, 6568.

Table 4. Electric and Magnetic Hyperfine Parameters of **3**: Comparison of B3LYP Values Computed at Four Different Geometries and Experimental Values[13]

	BP86-opt	B3LYP-opt	LDA-opt	X-ray structure	expt
δ (mm/s)	0.17	0.16	−0.01	0.02	0.13
ΔE_q (mm/s)	0.96	1.11	0.67	1.21	1.24
η	0.12	0.09	0.19	0.09	−
A^{iso} (^{57}Fe) (MHz)[a]	−20	−21	−26	−26	−20
A^{d} (^{57}Fe) (MHz)[a]	−8, −8, +16	−8, −8, +16	−9, −8, +17	−9, −8, +18	−11, −5, +16
A^{iso} (^{17}O) (MHz)	−17	−15	−17	−16	−
A^{d} (^{17}O) (MHz)[a]	−34, −31, +65	−34, −31, +65	−34, −31, +65	−36, −29, +65	−

[a] Isotropic contact term scaled with the factor 1.81 determined in ref 54. Both isotropic and anisotropic contributions contain spin−orbit coupling contributions.

realistic result. The $^5A_1$ and $^3A_2$ states are now calculated to be nearly degenerate, but the order relative to experiment[13,25] is still reversed.

As expected, the B3LYP value of 0.38 eV for the splitting between $^5A_1$ and $^3A_2$ for the BP86- or B3LYP-optimized structures is smaller than the value of 0.56 eV calculated by Decker et al.[25] using the BP86 functional, since the absence of Hartree−Fock exchange in BP86 favors low-spin states. The B3LYP calculations appear to give a reasonably realistic picture of the spin-state energetics in this case.

Mössbauer Properties. The calculated MB parameters are surprisingly sensitive to the geometry employed (Table 4). The calculated isomer shift δ varies between −0.01 and +0.17 mm/s, which bracket the experimental value[13] of 0.13 mm/s. The reason for this sensitivity is the steep dependence of the isomer shift on the iron−ligand bond distances.[34] Thus, the LDA structure strongly underestimates both the distance to the axial acetonitrile ligand (Table 2) and the isomer shift. The best value is obtained for the BP86- and B3LYP-optimized structures despite their significant error in the computed equatorial bond distances. This is, however, not surprising since the correlation between electron density at the iron nucleus and isomer shift has been made at theoretical geometries optimized using the BP86 functional.[34] The calculated quadrupole splitting ΔE_q also varies strongly with geometry and is underestimated in the calculations based on the LDA-optimized geometry. The calculations on both the experimental structure and the BP86- or B3LYP-optimized structures provide results in reasonable agreement with experiment. The calculated asymmetry parameter η is small as expected for a complex of effective C_{4v} symmetry. This is the case for mononuclear iron−oxo complexes where the bonding is strongly dominated by the strong Fe═O double bond with considerable anisotropic covalency.

Hyperfine Tensors. The calculated magnetic hyperfine tensor of the ^{57}Fe MB absorber is nearly axial and depends only to a limited extent on the particular structure. In a systematic study it was found that the complete ^{57}Fe hyperfine tensor can be fairly accurately predicted with the B3LYP method once the systematic error in the contact term is accounted for.[54] Thus, multiplication of the calculated contact term for ^{57}Fe by 1.81 and use of the dipolar and spin−orbit contributions as calculated by coupled perturbed B3LYP yield good predictions for a wide variety of valence and spin states of different iron complexes; scalar relativistic corrections using the zero-order regular approximation merely make the scaling factor a little smaller, but the overall quality of the correlation is not improved.[54] Accordingly, the present calculations yield a realistic ^{57}Fe tensor with the best agreement found for the BP86- and B3LYP-optimized structures. This is not surprising since the correlation was established for geometries optimized using the BP86 functional.[54] We note in passing that, as expected from the small anisotropy of the **g**-tensor, the SOC contribution to the HFC tensor is quite small (∼+0.6 MHz || to Fe═O and +1.3 MHz ⊥ to Fe═O based on the BP86-optimized structure), and consequently, the spin-dipolar term dominates the anisotropy in the HFC tensor.

Owing to the large spin density on the oxo group, the calculated values for the HFC tensor of ^{17}O are quite large and nearly structure-independent (Table 4). To the best of our knowledge, experimental values are not available for this quantity.

g- and D-Tensor. The **g**-tensor of **3** is comparable to that of the small model **2** with a small *g*-anisotropy: the calculated *g*-values are 2.015 (|| to Fe═O), 2.024, and 2.026 (⊥ to Fe═O). These *g*-values are much closer to the free electron value ($g_e = 2.002319$) than those quoted in the experimental article.[13] However, it must be emphasized that the experimental analysis is based on a ligand field model that assumes proportionality between the *g*-shift and the ZFS tensor.[55] This assumption is not generally valid, since only excited states of the same total spin ($\Delta S = 0$) contribute to the *g*-shift while states with $\Delta S = 0, \pm 1$ contribute to the **D**-tensor.[53] As pointed out for **2**, the **D**-tensor of the $(FeO)^{2+}$ unit has major contributions from the first low-lying $S = 2$ and $S = 0$ ligand field excited states, which are primarily responsible for the large positive value of the ZFS parameter *D*. Thus, the ligand field model is invalid in the present case, and therefore a reliable experimental value for the **g**-tensor of the $(FeO)^{2+}$ unit is still lacking.

The calculated ZFS tensor is qualitatively similar to the one calculated for the small model **2**. Since the experimentally determined ZFS value is extremely large, we consider it likely that higher than second-order terms may contribute to the ZFS. Nevertheless, our second-order results are collected in Table 5. The BP86-calculated values are reasonable but clearly underestimate the *D*-value. The individual contributions to the *D*-value are very similar to those discussed for the small model **2**. In the Supporting Information we give a semiquantitative estimate estimate of the *D*-value based on a ligand field model that predicts a *D*-value of +22.5 cm^{-1} if the low-lying quintet state is assumed to be at ∼0.3 eV above the $^3A_2$ ground state. In this model, the quintet state makes the largest contribution (∼15 cm^{-1}). A comparison with the results from the quasi-restricted DFT approach indicates that the latter fails to provide sufficiently accurate energy denominators. This is particularly true for the energies of the spin-forbidden excitations which are poorly estimated in the quasi-restricted scheme.

(54) Sinnecker, S.; Slep, L.; Bill, E.; Neese, F. *Inorg. Chem.* **2005**, *44*, 2245.

(55) Oosterhuis, W. T.; Lang, G. *J. Chem. Phys.* **1973**, *58*, 4757.

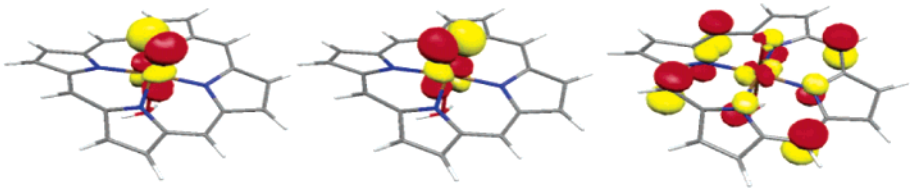

Figure 3. Essentially singly occupied natural orbitals of the DDCI2 wave function for **5** in the quartet ground state.

Table 5. ZFS Parameters for **3**: Comparison of BP86 Values Computed at Four Different Geometries and Experimental Values[13,18]

	BP86-opt	B3LYP-opt	LDA-opt	X-ray structure	expt
D (cm^{-1})	+12.0	+13.0	+11.5	+12.3	+26,[a] +29[b]
E/D	0.01	0.01	0.0	0.0	small

[a] MCD study.[25] [b] MB study.[13]

C. Studies on Fe(TPP)═O Models. As the next step in calibration, we have studied two oxo porphyrin radical models spectroscopically characterized by Weiss, Trautwein, Bill, and co-workers.[14] These model complexes show reasonably strong ($J = 38-43$ cm^{-1}) ferromagnetic coupling between the spins of the FeO unit ($S_{FeO} = 1$) and the porphyrin ($S_{P\bullet} = {}^1/_2$) resulting in a quartet ground state ($S_t = {}^3/_2$). This is in contrast to all calculations on computational models for the actual Compound I, which predict an antiferromagnetically coupled doublet ground state[56] with potentially important consequences for multistate reactivity.[5] However, the previously published conclusions are based on single-determinantal BS-DFT calculations, which are incapable of providing a proper description of the low-spin (doublet) state. It is therefore desirable to extend the calculations to the multireference ab initio domain.

Unfortunately, crystal structures of these complexes are not available. Since it is not known from experiment whether the studied complexes possess an axial ligand, we have constructed two models, without (**4**) and with (**5**) a water ligand in the axial position (Table 6).

Geometries. The geometries of both models were optimized in the quartet state using the B3LYP functional and the SV(P) basis set. Truncated models (**6** and **7**) were constructed from the optimized structures by replacing the phenyl substituents with hydrogen atoms in a standard geometry. Both systems exhibit the expected short Fe═O bond (1.612 Å in **5** and 1.596 Å in **4**) in reasonable agreement with the value of 1.64 Å derived from extended X-ray absorption fine structure (EXAFS) measurements.[57,58] The axial water in **5** stays bound, although at a fairly long distance of 2.17 Å in our calculations, which would have been difficult to detect by EXAFS.

Exchange Coupling. In addition to the DFT calculations of the magnetic coupling parameters, we have also carried out correlated ab initio calculations on the exchange coupling parameter (using $\hat{H}_{HDvV} = -2J\vec{S}_A\vec{S}_B$) at the DDCI2 level as described under Computational Details. These calculations have the advantage that they yield pure spin eigenfunctions and are therefore expected to be more reliable than the BS-DFT approach. The reference space for the DDCI2 calculations had to be kept at a minimum to stay tractable. It is evident that the

Table 6. B3LYP/SV(P)-Optimized Geometries of the Iron−Oxo *meso*-Tetraphenyl Model Compounds **4** and **5** in the Quartet State[a]

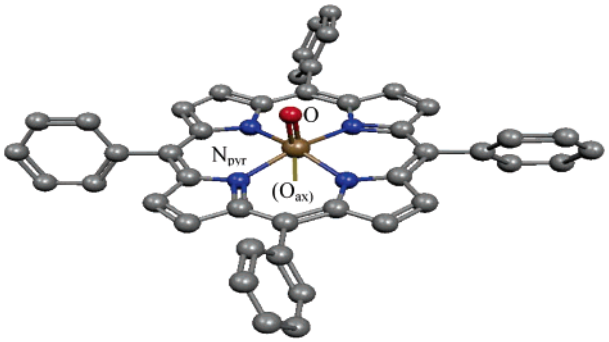

	4	5
R(Fe═O)	1.596	1.612
R(Fe−O_{ax})	−	2.168
R(Fe−N_{pyr})[b]	2.029	2.039
α(N−Fe−N)[b]	89.0	89.4

[a] The calculated geometry of the BS doublet species is virtually identical. Distances R in Å, angle α in degrees. [b] Averaged value.

spin density of the Fe^{IV}═O unit is located in the two singly occupied FeO−π^* orbitals, which therefore must be in the active space. On the porphyrin, two alternative SOMOs exist that are usually classified as a_{1u} and a_{2u} under effective D_{4h} symmetry.[59] In our calculations, it is the a_{2u} (Figure 3) orbital that is singly occupied in accord with the DFT results and experiment.[14,58] This choice results in a minimal active space of three electrons in three orbitals (CAS(3,3)) which was later also chosen for Compound I.

Our best estimate[60] for the doublet−quartet splitting of the six-coordinate (6C) species **5** is 208 cm^{-1}, which corresponds to a ferromagnetic exchange coupling of $J = +69$ cm^{-1}. This number can be compared with the experimental estimates of 38−45 cm^{-1} and the B3LYP prediction of +116 cm^{-1}. For the five-coordinate (5C) species **4**, the DDCI2 calculations predict a small antiferromagnetic coupling ($J = -25$ cm^{-1}), while the B3LYP prediction stays ferromagnetic ($J = +57$ cm^{-1}). Thus, the B3LYP method predicts more positive values than the DDCI2 method.

Spin Densities. For **5** (**4**) the calculated Löwdin spin populations at the B3LYP level in the quartet ground state are 1.20 (1.26) on Fe and 0.87(0.78) on the oxo ligand, indicating a slightly higher oxo-to-iron charge donation in **5** compared to **4** or the non-heme model **3**. Again, the agreement with the

(56) Ogliaro, F.; de Visser, S. P.; Cohen, S.; Kaneti, J.; Shaik, S. *ChemBioChem* **2001**, *2*, 848.
(57) Penner-Hahn, J. E.; Eble, K. S.; McMurry, T. J.; Renner, M.; Balch, A. L.; Groves, J. T.; Dawson, J. H.; Hodgson, K. O. *J. Am. Chem. Soc.* **1986**, *108*, 7819.
(58) Fujii, H. *Coord. Chem. Rev.* **2002**, *226*, 51.
(59) Terner, J.; Gold, A.; Weiss, R.; Mandon, D.; Trautwein, A. X. *J. Porphyrins Phthalocyanines* **2001**, *5*, 357.
(60) To prove that our individually selecting MR−CI program is indeed providing converged results for the doublet−quartet splitting, the doublet−quartet gap has been computed as a function of the selection threshold $T_{sel} = 10^{-n} E_h$ ($n = 5, 6, ..., 10$), which yields gaps of 1915, 565, 272, 217, 206, and 208 cm^{-1}, respectively. It is evident that the splitting is a sensitive function of the selection threshold and requires tight values for convergence.

Table 7. Calculated MB Parameters and ^{57}Fe as Well as ^{17}O Hyperfine Coupling Constants (B3LYP level) for the Quartet Ground States of Untruncated 5C and 6C Models in Comparison with Experimental Results for Two Closely Related Model Complexes

	5C species, **4**	6C species, **5**	expt
δ (mm s^{-1})	0.08	0.11	0.06,[a] 0.08[b]
ΔE_q (mm s^{-1})	2.21	1.16	1.48,[a] 1.62[b]
η	0	0	0,[a] 0[b]
A^{iso} (^{57}Fe) (MHz)	−18[c]	−18[c]	−18.3,[a] −18.3[b]
$A_{x,y}^{d}$(^{57}Fe) (MHz)	−6.5	−5.9	−8.5,[a] −9.2[b]
A_z^{d}(^{57}Fe) (MHz)	13.0	11.7	17.0,[a] 18.4[b]
A^{iso} (^{17}O) (MHz)	−11.2	−12.3	−
$A_{x,y}^{d}$ (^{17}O) (MHz)	−20.1	−22.6	−
A_z^{d} (^{17}O) (MHz)	40.3	43.8	−

[a] [FeO(TDCPP)]$^+$, ref 14. [b] [FeO(TMP)]$^+$, ref 14. [c] Contact contribution scaled with the factor 1.81 determined in ref 54. Both isotropic and anisotropic values contain spin−orbit coupling contributions.

DDCI2 values of 1.11 (1.13) on Fe and 0.87 (0.83) on O is reasonable. Evidently the highly covalent $(FeO)^{2+}$ core is not grossly perturbed in a heme environment compared to a non-heme one. In all cases, the spin density on the $(FeO)^{2+}$ unit is approximately two unpaired electrons. The third unpaired electron is located on the porphyrin ring with high spin densities at the methine bridges (∼0.23). In the B3LYP calculations, the pyrrole nitrogens also receive significant spin populations (∼0.1 electron each), which are compensated by some negative spin populations throughout the ring system.

Mössbauer Parameters. The calculated MB parameters for **4** and **5** are shown in Table 7. Both models give reasonable agreement with the experimentally determined isomer shifts δ, which consequently do not allow us to discriminate between the two alternatives. However, the quadrupole splitting ΔE_q for **4** is predicted to be very large, as might be expected for a 5C species with approximate C_{4v} symmetry. It is more than 0.5 mm s^{-1} larger than the experimentally determined value. This deviation would appear to be outside the error bounds of the DFT methods used for the prediction of quadrupole splittings.[61] Thus, the calculations favor **5** as the experimentally observed species. As found for the model complex **3**, the predicted ^{57}Fe HFCs are of excellent quality after scaling is applied to the contact part and SOC contributions are taken into account. In this case, both **4** and **5** have similar HFC values.

EPR Parameters. Since the **g**-tensor of a porphyrin radical will reflect that of a typical organic radical with small deviations from the free electron *g*-value, one may neglect the contribution of the porphyrin radical to the *g*-shift Δg.[62] Thus, $\Delta g_{3/2}$ is expected to be equal to $^2/_3\Delta g_{FeO}$, while that of the doublet state should equal $^4/_3\Delta g_{FeO}$ (based on standard spin-coupling algebra[43]). Our calculations indeed predict *g*-shifts on the order of 0.01 with limited rhombicity, and therefore they closely parallel the results obtained for the $(FeO)^{2+}$ model systems. Again, this deviates from the "experimental" numbers.[14] However, the experimental analysis is inflicted with the same problem as in the case of the model compound **3** in the previous section.

Table 8. Calculated Intrinsic Zero-Field Splitting Parameters for the $(FeO)^{2+}$ Unit of **6** and **7** (BP86 level)

	5C species, **6**	6C species, **7**	expt[a]
D (cm^{-1})	−19.6	8.5	+18
E/D	0.11	0.19	<0.1

[a] MB study, ref 14.

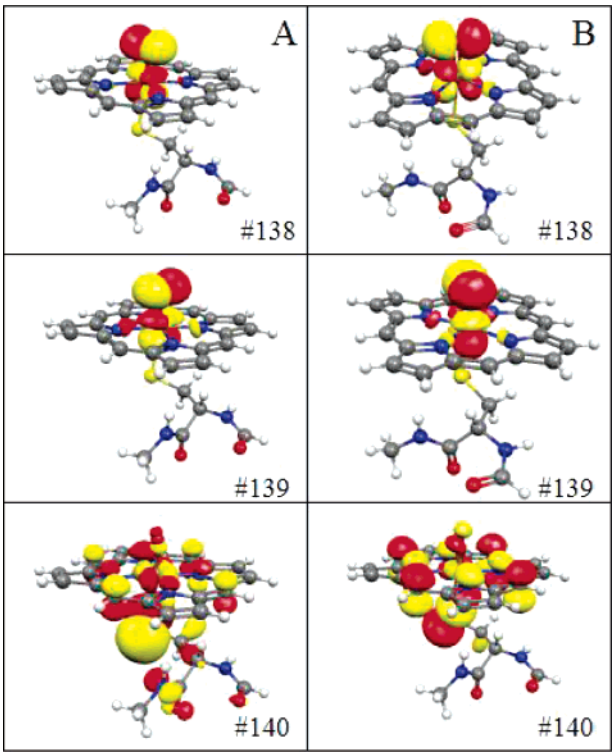

Figure 4. Singly occupied spin-unrestricted natural orbitals (^{4}A state) of the Compound I model **1** without the external field (A) and in the field of the protein point charges (B).

Consequently, a reliable experimental number is not available. However, since the **g**-tensor is almost isotropic and close to the free electron *g*-value, it will not have a pronounced influence on the shape of the EPR spectrum compared to the combined effects of exchange coupling and zero-field splitting.

Much more important is the computed ZFS tensor of the quartet state (Table 8), which dominates the EPR spectrum.[14] The calculated **D**-tensor of the $S_t = {}^3/_2$ state was multiplied by the factor of 3 to account for the spin coupling between the $(FeO)^{2+}$ core and the porphyrin radical to give a value of 8.5 cm^{-1} for D_{FeO} in the 6C case but a *negative* value of −19.6 cm^{-1} for the 5C case. Since the experimentally determined ZFS is positive,[14] these calculations again favor the formulation of the observed species as **5**. The quantitative accuracy of the DFT values is limited with the error exceeding a factor of 2 in this case. In addition, the calculations predict an intermediate rhombicity that is not observed experimentally.

D. Results for Compound I in the Protein Matrix. Electronic Structure and MO Populations. The singly occupied natural orbitals from spin-unrestricted DFT calculations on model **1** for Compound I are shown in Figure 4 without (Figure 4A) and with (Figure 4B) the polarizing field of the protein point charges. It is observed that two of the natural orbitals (#138 and #139) closely resemble the two π*-SOMOs of the $(FeO)^{2+}$ unit and change very little upon embedding of **1** in the protein matrix. However, as discussed previously,[16] the

(61) Godbout, N.; Havlin, R. H.; Salzmann, R.; Debrunner, P. G.; Oldfield, E. *J. Phys. Chem. A* **1998**, *102*, 2342.
(62) The calculated *g*-values of [Zn(porphyrin)]$^+$ using the BP86 functional are 2.003 ($g_\perp$) and 2.012 ($g_\parallel$). Experimentally, this species shows *g*-values that depend markedly on the environment of the radical and vary between 2.004 and 2.01 and thus confirm our statement. See, for example: (a) Dave, P. C.; Srivinas, D. *J. Porphyrins Phthalocyanines* **2000**, *4*, 192. (b) Dave, P. C.; Srivinas, D. *J. Porphyrins Phthalocyanines* **1997**, *2*, 243 and references therein.

Table 9. Calculated Principal g-Values and Heisenberg Exchange Coupling Constant J (cm^{-1}) for Compound I of $P450_{cam}$ at the B3LYP Level[a]

state	system	g	J/cm^{-1}
^2A	S_p	2.016, 2.009, 1.982 (2.020, 2.012, 1.918)[b]	−16
	S_g	2.015, 2.008, 1.980 (2.020, 2.007, 1.916)[b]	−27
^4A	S_p	2.045, 2.012, 2.006	
	S_g	2.045, 2.013, 2.006	−

[a] S_p refers to the system in the enzyme environment, S_g to the system in the gas phase. [b] Spin-projected values (in parentheses).

third natural orbital with unit occupation (#140), which represents the porphyrin hole, changes significantly in the protein environment. In the gas-phase calculations (Figure 4A), the orbital is mainly located on the axial thiolate ligand, while in the protein (Figure 4B) it is essentially a porphyrin a_{2u}-like orbital. By the same time, the sulfur contribution changes from predominantly π-type to pseudo-σ-type, which shows that the protein affects the orientation of the sulfur lone pair orbital. On a more quantitative level, the Löwdin population analysis shows a decrease of the sulfur spin population by more than a factor of 2 (from 0.60 to 0.28) when going from vacuum to the protein environment, while the iron (1.17 → 1.19) and oxo (0.88 → 0.85) spin populations stay almost invariant.

Exchange Couplings. Calculated Heisenberg exchange coupling constants for the exchange coupled system are given in Table 9, together with g-values. Previous QM/MM calculations[16] with the same QM region and a smaller basis set predicted the antiferromagnetic doublet to be the ground state, being more stable than the quartet state by only 11 cm^{-1} ($J = -4$ cm^{-1}).[16] This assignment is confirmed by the present single-point calculations that employ a larger basis set (TZVP) and lead to similar values, J being -16 cm^{-1}. In the gas-phase calculations, we obtain a coupling constant of $J = -27$ cm^{-1}. This value may be compared to the experimental datum of -37 cm^{-1} for Compound I in chloroperoxidase.[63] Likewise, J is also negative, but smaller in Compound I of horseradish peroxidase.[64] Our calculations thus correctly reproduce the intriguing experimental finding that the sign of J is reversed in the native Compound I species as opposed to Compound I model complexes, like the ones discussed above, which all show ferromagnetic coupling. Weiss et al. suggested[65] that this effect is a result of the delocalization of one oxidizing equivalent not only over the porphyrin, but also over the proximal axial ligand. Specifically, interactions of orbitals on sulfur and the oxoferryl moiety are thought to provide the overlap of magnetic orbitals that would give rise to the observed antiferromagnetic coupling. Similar ideas have also been brought forward by Green on the basis of DFT calculations.[20]

For Compound I model **1** in the presence of the protein point charges (S_p), the DDCI2 treatment yields an antiferromagnetic doublet−quartet splitting of -39.2 cm^{-1} corresponding to an exchange coupling parameter of $J \approx -13$ cm^{-1}, which is in excellent agreement with the B3LYP value. Despite repeated attempts, a suitable spin-restricted reference state as input for the correlated calculation could not be obtained for **1** in the absence of the point charges.

Table 10. Calculated MB Isomer Shift $\delta(^{57}Fe)$, Quadrupole Splitting ΔE_q, and Asymmetry Parameter η for Compound I of $P450_{cam}$[a]

spin state	system	ΔE_q/mm s^{-1}	η	$\delta(^{57}Fe)$/mm s^{-1}
^2A	S_p	0.67	0.09	0.13
	S_g	1.34	0.06	0.09
^4A	S_p	0.64	0.10	0.13
	S_g	1.33	0.03	0.09

[a] S_p refers to the system in the enzyme environment, S_g to the system in the gas phase.

The spin populations calculated at the DDCI2 level for the quartet state are almost identical to the ones from the B3LYP-DFT calculations. However, the spin populations of the doublet ground state necessarily differ substantially due to the multiconfigurational character of the doublet state that cannot be described properly by broken symmetry DFT. The DDCI2 spin populations on Fe, O_{oxo}, S, and the pyrrole nitrogens (average) are 0.75, 0.54, −0.08, and −0.03, respectively, which are all substantially lower than the B3LYP values of 1.30, 0.79, −0.30, and −0.13. Thus, the broken symmetry solution as such can certainly not be used to calculate spin-dependent properties of Compound I, and one needs to at least apply spin projection to arrive at reasonable properties from DFT (as has been done for all spectroscopic properties as described in the Supporting Information, but not for the populations).

Coupling to the $S_{FeO} = 2$ State. Since the calculations on the $(FeO)^{2+}$ core on **2** and **3** revealed the importance of the first low-lying quintet state, we have also considered the possibility of coupling this state to the porphyrin radical (Scheme 2). Ferromagnetic coupling gives a total spin of $S_t = {}^5/_2$, while antiferromagnetic coupling results in $S_t' = {}^3/_2$ but with a different orbital occupation pattern compared to the $S_t = {}^3/_2$ ground state. The coupling of the local quintet state of the $(FeO)^{2+}$ unit with the porphyrin radical was studied at the B3LYP level for both **1**(S_p) and **1**(S_g). The corresponding results on models **6** and **7** are documented in the Supporting Information, while those for **1** are given here.

In the gas phase, the sextet state is calculated to be 0.64 eV above the ground state in **1**(S_g) and is coupled by a small antiferromagnetic J of -38 cm^{-1} to the porphyrin radical. The protein effect is moderate: for **1**(S_p), the sextet state of is calculated to be 0.52 eV above the ground state, and the antiferromagnetic coupling decreases to -26 cm^{-1}. These results show that there is a manifold of states in Compound I, within ~12 kcal/mol of the ground state, which differs qualitatively in the orbital occupation pattern. While it appears unlikely that this manifold becomes the ground state, it may play a role as the system moves toward a transition state. This needs to be investigated more closely in future work.

Mössbauer Parameters. The calculated MB data for Compound I of $P450_{cam}$ are collected in Table 10. We compare the parameters from the QM/MM treatment in the enzyme environment (S_p) to those of isolated system in the gas phase (S_g). The gas-phase results are very similar to those obtained for the model complexes **4** and **5** (section C). Comparing only the equivalent quartet states, the quadrupole splitting (isomer shift) is 1.34 (0.09) mm s^{-1} as compared to 1.48 (0.06) mm s^{-1} in **4** and 1.62 (0.08) mm s^{-1} in **5**. The spectral features of Compound I are, however, significantly changed in the enzyme environment: ΔE_q is reduced to 0.64 mm s^{-1} and $\delta(^{57}Fe)$ is increased

(63) Rutter, R.; Hager, L. P.; Dhonau, H.; Hendrich, M.; Valentine, M.; Debrunner, P. *Biochemistry* **1984**, *23*, 6809.
(64) Schultz, C. E.; Rutter, R.; Sage, J. T.; Debrunner, P. G.; Hager, L. P. *Biochemistry* **1984**, *23*, 4743.
(65) Weiss, R.; Mandon, D.; Wolter, T.; Trautwein, A. X.; Müther, M.; Bill, E.; Gold, A.; Jayaraj, K.; Terner, J. *J. Biol. Inorg. Chem.* **1996**, *1*, 377.

Scheme 2

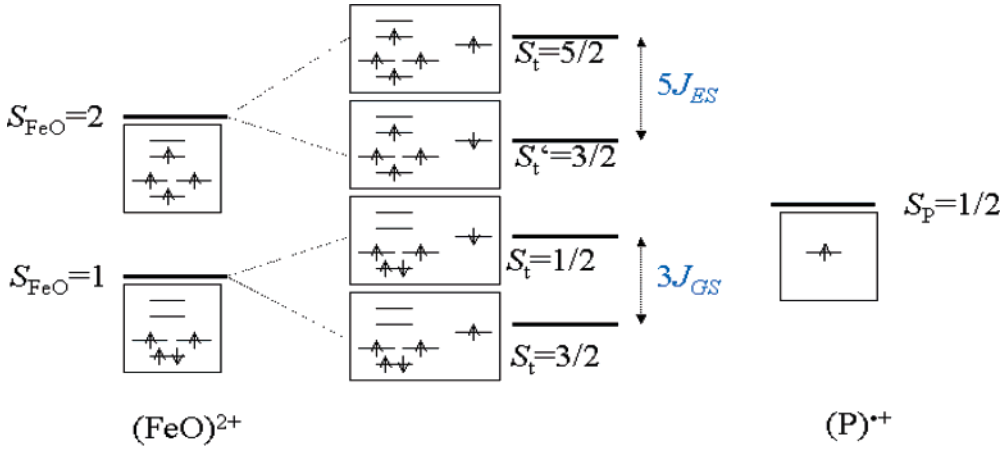

Table 11. Calculated Intrinsic Zero-Field Splitting Parameters for the $(FeO)^{2+}$ Unit of **1** (BP86 level)[a]

	$^4A, S_p$	$^4A, S_g$
D (cm^{-1})	24.9	33.6
E/D	0.32	0.27

[a] Note that the ZFS of the $S_t = {}^3/_2$ state is obtained by division of D and E by 3.

to 0.13 mm s^{-1}, which indicates a decrease of charge at the iron nucleus in the protein. In fact, all iron−ligand bonds except for the already fairly long Fe−S bond become slightly longer in the protein environment, which may serve to explain this effect.[16] The quartet and doublet states exhibit nearly identical MB parameters. This is reasonable because they depend only on the total electron density, which is very similar in both spin states. Note also that, for the doublet state, no spin projection is necessary in the case of MB parameters since the broken symmetry formalism is expected to yield reasonable electron densities but unphysical spin densities.

Zero-Field Splittings. The ZFS values obtained for **1** are collected in Table 11. The calculated ZFS is larger than that for the model compounds **4**−**6** and more in line with the results typically found in experiments on iron−oxo porphyrins.

The effect of the protein matrix is significant: the ZFS is reduced by ∼40%. This may be rationalized by the altered spin distribution in the protein environment. Thus, spin density is taken away from the thiolate ligand, which may significantly contribute to the SOC effects in the quartet state. Surprisingly, the calculated ZFS tensor is almost perfectly rhombic, in which case the sign of D becomes insignificant. This result is consistent with a low electronic symmetry in Compound I. Apparently the axial contribution of the $(FeO)^{2+}$ unit to the ZFS is altered by the presence of the porphyrin hole such that the principal axes system is significantly rotated.

***g*-Shifts.** The g-shifts computed for Compound I are rather small, similar to the situation in the model complexes discussed above. However, in going to the cysteinate ligated system, there is a slight tendency toward a nonaxial pattern. In particular, there is now one g-shift predicted that is significantly below the free electron g-value from the doublet state species, pointing to the presence of a low-lying unoccupied spin-down level which is available for efficient SOC. Nevertheless, the effects of g-anisotropy on the shape of the spectrum will remain limited owing to the competing ZFS and exchange interactions. No significant changes in the g-values are observed between the isolated gas-phase system (S_g) and the system in the enzyme environment (S_p).

Hyperfine Couplings. Table 12 summarizes the calculated hyperfine coupling constants on the ferryl atom, as well as on the oxo and pyrrole nitrogen ligands. Comparing again the data on the quartet with those for the synthetic compounds **4** and **5** (Table 7), it is obvious that the overall features of the hyperfine tensor are very similar in these compounds. Thus, the HFCs of both the central iron atom and the oxo ligand are the same to within a few megahertz.

Comparing the theoretical results for the doublet ground state with those for the quartet state (Table 12), the metal and oxo HFCs appear to have enhanced hyperfine interactions that are mainly due to the spin projection coefficient of ${}^4/_3$ for the majority spin fragment in the spin-coupled system. The HFCs of the ligand nuclei on the minority spin fragment change sign and are of similar magnitude for the doublet and quartet states. Qualitatively, the resonance patterns are, however, very similar.

It is noted that the ^{15}N−HFCs for Compound I are different from those of the resting state which have been measured to be 5−6 MHz, in agreement with preliminary calculations.[66] In Compound I, the dipolar part prevails over the isotropic contact contribution. Thus, the ^{14}N ENDOR signals are a potentially valuable source of information for Compound I should it become amenable to experimental study. The relatively large dipolar couplings are explained by the large out-of-plane spin density in the π^*-orbitals of the $(FeO)^{2+}$ unit which will strongly interact with the p_z orbitals of the nitrogen donors and thereby induce the rather large calculated dipolar couplings (cf. Figure 4, orbital #140).

The largest hydrogen HFCs of Compound I are listed in Table 13. The most notable interaction is found with the β-hydrogen atoms on the cysteinate ligand, one of which shows isotropic coupling constants of (S_p/S_g) −8/−17 MHz and 6/16 MHz in the ^2A and ^4A states, respectively. These couplings are a sensitive reporter of the spin density on the adjacent sulfur atom as has been worked out in great detail for type I[67] and Cu_A[68]

(66) Schöneboom, J. Ph.D. Thesis, Universität Düsseldorf, Düsseldorf, Germany, 2003.
(67) Werst, M. M.; Davoust, C. E.; Hoffman, B. E. *J. Am. Chem. Soc.* **1991**, *113*, 1533.
(68) (a) Neese, F.; Kappl, R.; Zumft, W. G.; Hüttermann, J.; Kroneck, P. M. H. *J. Biol. Inorg. Chem.* **1998**, *1*, 53. (b) Epel, B.; Slutter, C.; Neese, F.; Kroneck, P. M. H.; Zumft, W. G.; Pecht, I.; Farver, O.; Lu, Y.; Goldfarb, D. *J. Am. Chem. Soc.* **2002**, *124*, 8152.

Table 12. Calculated ^{57}Fe, ^{17}O, and ^{14}N Hyperfine Coupling Constants (MHz) in Compound I for the ^{2}A and ^{4}A States from B3LYP Calculations[a,b]

		^{2}A state[c]		^{4}A state				^{2}A state[c]		^{4}A state	
		S_p	S_g	S_p	S_g			S_p	S_g	S_p	S_g
Fe	A^{iso}	−28.5[e]	−29.4[e]	−17.8[e]	−17.7[e]	N^B	A^{iso}	−2.1	−0.3	1.8	1.2
	A_x[d]	−14.0	−13.3	−6.0	−5.9		A_x[d]	2.1	1.2	−2.1	−1.1
	A_y[d]	−13.2	−13.0	−5.6	−5.7		A_y[d]	1.5	0.5	−1.5	−0.4
	A_z[d]	23.3	22.5	11.7	11.6		A_z[d]	−3.6	−1.6	3.6	1.6
O[d]	A^{iso}	−21.5	−21.7	−12.5	−11.7	N^C	A^{iso}	−1.9	−0.5	3.0	2.4
	A_x[d]	−43.9	−43.5	−20.5	−20.4		A_x[d]	2.1	1.4	−2.2	−1.4
	A_y[d]	−40.6	−41.3	−18.4	−19.6		A_y[d]	1.5	0.7	−1.4	−0.6
	A_z[d]	84.5	84.8	38.9	40.0		A_z[d]	−3.6	−2.1	3.6	2.0
N^A	A^{iso}	−1.8	−0.6	2.4	1.9	N^D	A^{iso}	−2.7	−3.6	2.4	5.0
	A_x[d]	1.3	0.6	−2.0	−1.3		A_x[d]	2.3	2.4	−2.3	−2.5
	A_y[d]	1.9	1.3	−1.3	−0.5		A_y[d]	1.7	1.8	−1.7	−1.7
	A_z[d]	−3.2	−1.9	3.2	1.9		A_z[d]	−4.0	−4.2	4.0	4.2

[a] S_p refers to the system in the enzyme environment, S_g to the system in the gas phase. [b] For explanation of the labels N^A−N^D see inset in Scheme 1. [c] Spin-projected values. [d] Oxo ligand. [e] Contact term scaled by 1.81 according to ref 54.

Table 13. Calculated ^{1}H Hyperfine Coupling Constants (MHz) Compound I for the ^{2}A and ^{4}A State (B3LYP Level)[a]

		^{2}A state[b]		^{4}A state				^{2}A state[b]		^{4}A state	
		S_p	S_g	S_p	S_g			S_p	S_g	S_p	S_g
H^{β}_1	A^{iso}	−7.6	−17.0	6.4	16.4	H^{meso}_2	A^{iso}	3.6	1.9	−3.6	−1.8
	A_x[d]	−0.6	−1.1	−1.1	−1.4		A_x[d]	−1.7	−0.7	−3.0	−1.8
	A_y[d]	0.0	−0.0	−0.6	−0.8		A_y[d]	−0.2	−0.0	−0.7	−0.6
	A_z[d]	0.6	1.1	1.7	2.2		A_z[d]	1.9	0.8	3.6	2.4
H^{β}_2	A^{iso}	−2.7	−6.8	1.9	6.1	H^{meso}_3	A^{iso}	3.6	2.0	−3.7	−2.0
	A_x[d]	−1.1	−1.7	−1.5	−1.7		A_x[d]	−1.8	−0.9	−3.1	−2.0
	A_y[d]	−0.5	−0.0	−1.0	−0.7		A_y[d]	−0.1	−0.0	−0.7	−0.6
	A_z[d]	1.5	1.7	2.5	2.4		A_z[d]	2.0	0.9	3.8	2.6
H^{meso}_1	A^{iso}	3.4	1.9	−3.4	−1.9	H^{meso}_4	A^{iso}	3.2	1.8	−3.2	−1.8
	A_x[d]	−1.6	−0.9	−2.8	−1.9		A_x[d]	−1.4	−0.8	−2.8	−1.8
	A_y[d]	−0.1	0.1	−0.7	−0.6		A_y[d]	−0.2	0.1	−0.7	−0.6
	A_z[d]	1.7	0.8	3.4	2.5		A_z[d]	1.6	0.7	3.4	2.4

[a] S_p refers to the system in the enzyme environment, S_g to the system in the gas phase. [b] Spin-projected values.

copper centers. They also show a pronounced dependence on the H−C−S−Fe dihedral angle, which is potentially very useful for conformational analysis. The large difference (>factor 2) between the gas-phase (S_g) and protein (S_p) results can be attributed to the fact[16] that the spin density on the sulfur drops by almost a factor of 2 upon explicit modeling of the protein with the QM/MM approach. Thus, in the gas-phase calculations Compound I appears as a sulfur radical-like species, while in the protein environment most of the ligand spin density is shifted to the porphyrin ring. This is attributable to the polarizing effect of the protein environment which reduces the donor capability of the cysteinate ligand.[16] The large changes occurring in the ligand spin density distribution are nicely reflected in the strong isotropic (and anisotropic) HFCs of the cystein H_β protons, which should be a prime target for ENDOR analysis of Compound I.

The other significant couplings arise from the *meso*-hydrogen atoms, which have resonances in the range of ±(2−6) MHz in the ^{2}A and ^{4}A states. These HFCs are also very sensitive to environmental factors. They become larger when moving from the gas phase to the protein because the porphyrin radical character increases dramatically upon inclusion of the protein environment. Thus, there is a concentration of spin density in the p-orbitals at the *meso*-carbon atoms, which contribute to the singly occupied a_{2u} orbital. Hence, analogous to the calculated MB data, accounting for the steric and electronic influence of the protein environment leads to non-negligible effects on the spectral features.

4. Discussion and Conclusions

In the present study we have predicted a fairly complete set of magnetic spectroscopic parameters (EPR, ENDOR, and MB) of the elusive Compound I species in cytochrome $P450_{cam}$ in the presence of the protein matrix using density functional theory and correlated ab initio methods. The calculations have been calibrated on experimentally known species and on small hypothetical models where higher level calculations can be done. The ultimate goal of this contribution is to provide a set of calibrated spectroscopic parameters that may be used to identify Compound I in future experimental investigations.

To the best of our knowledge, this is also the first time that QM/MM methods have been combined with DFT for the calculation of EPR spectroscopic parameters and also the first time that correlated ab initio theory has been applied to a large open-shell transition metal complex in the presence of a protein matrix. The most important conclusions of the present study may be summarized as follows.

The magnetic response of Compound I and related species is dominated by the combination of the reasonably weak exchange coupling between the porphyrin cation radical and the $(FeO)^{2+}$ unit as well as the large and positive ZFS of the $(FeO)^{2+}$ core. The exchange coupling of Compound I is consistently calculated to be small and negative. At the highest level available to us (DDCI2), a coupling constant of $J = -13$ cm^{-1} is obtained, leading to the prediction of the quartet state being only 39 cm^{-1} above the doublet ground state. Thus, this

state should be populated even at low temperatures (~77 K) in magnetic resonance or MB experiments, while at cryogenic temperatures (~4 K) the system should quantitatively reside in the doublet (antiferromagnetic) state. The DFT (B3LYP) prediction of $J = -16$ cm^{-1} is in excellent agreement with the ab initio value.

The ZFS of Compound I was found to be larger than that of comparable model systems by a factor of 2 or more. Since the quasi-restricted BP86 method used in this work tends to underestimate the value of D, we conservatively estimate the intrinsic ZFS of the $(FeO)^{2+}$ unit in Compound I to be $>+20$ cm^{-1}. The ZFS tensor was calculated to be nearly rhombic so that the sign of D becomes insignificant.[69] The combination of a large ZFS and a small J-value leads to the conclusion that the low-lying doublet and quartet states will be heavily mixed such that the notion of a well-defined ground-state multiplicity partially loses its meaning. If the values $J = -13$ cm^{-1}, $D_{FeO} = 24.9$ cm^{-1}, and $E/D = 0.32$ are inserted in the spin Hamiltonian $\hat{H} = -2J\hat{S}_{FeO}\hat{S}_P + D_{FeO}\lfloor \hat{S}^2_{z;FeO} - {}^2/_3 \rfloor + E_{FeO}\lfloor \hat{S}^2_{x;FeO} - \hat{S}^2_{y;FeO} \rfloor$, the resulting three Kramers doublets are located at 0, 36.4, and 57.8 cm^{-1}, respectively. They have $\langle S^2 \rangle$ values of 1.05, 3.56, and 3.63, respectively, and are thus already far from representing pure spin states.[70] The Boltzmann population of the lowest Kramers doublet is 100% at 4 K, ~54% at 77 K, and ~38% at 298 K. Thus, at ambient temperature, the three Kramers doublets have almost equal populations and may serve as starting point for reactions. That such a scenario is realistic follows from the classic experimental and theoretical work of Debrunner and co-workers on the spin-Hamiltonian parameters of Compound I species.[63,64,71] Thus, for horseradish peroxidase $D = 22.2$ cm^{-1} was found ($E/D \approx 0$) together with a very small and anisotropic $2J \approx -2$ cm^{-1}. For chloroperoxidase, Debrunner and co-workers determined $D = 35.8$ cm^{-1} ($E/D \approx 0$) and a ratio $|2J/D| \approx 1.02$, which comes reasonably close to the values calculated for $P450_{cam}$ in this work.

The hyperfine and superhyperfine couplings of Compound I were found to be sensitive reporters of the Compound I species itself and its geometric and electronic structure: (a) the ^{57}Fe hyperfine and ^{17}O hyperfine interactions are expected to be similar to those of model iron−oxo porphyrins, (b) the cysteine β-protons are predicted to show large couplings in the 20 MHz range, which will depend on the spin density at sulfur and hence its radical character as well as the conformation of the cysteine side chain, and (c) likewise both the ^{14}N pyrrole and the ^{1}H meso-protons are expected to show quite large couplings that are characteristic of the porphyrin radical character in Compound I and its spin distribution. The ^{14}N couplings are quite unusual in that they are dominated by a large dipolar part and a much smaller isotropic contribution which is attributed to the π-interactions between the spin-carrying $(FeO)^{2+}$ core and the out-of-plane p_z orbitals of the nitrogens. The meso-protons respond most sensitively to the a_{2u} porphyrin radical character, which is strongly influenced by the protein environment. The effects of the protein matrix on the spectroscopic parameters are clearly visible in our results and can be quite dramatic. As the protein environment strongly controls the spin distribution between the axial sulfur ligand and the porphyrin ring, a number of spectroscopic features respond sensitively to the presence of the protein environment. These are especially the ligand hyperfine couplings, but the MB properties and ZFS values are also significantly influenced.

In agreement with other studies,[16,44,72,73] MB parameters are reliably predicted by DFT methods for the type of species considered. Our results for the Compound I in the protein matrix indicate an isomer shift that is on the high side for a high-valent species (0.13 mm/s) and a quadrupole splitting that is on the low side (0.64−0.67 mm/s), with both values being essentially independent of the overall spin state being $S_t = {}^1/_2$ or $S_t = {}^3/_2$. The protein effect on both quantities is significant: the quadrupole splitting is distinctly lowered by the interaction with the protein environment while the isomer shift is increased. This is associated with a slight lengthening of all metal−ligand bonds except the Fe−S bond which is already long.

The $(FeO)^{2+}$ unit will usually have a $S = 1$ ground state as has been observed for most, but not all,[48] $(FeO)^{2+}$ species to date. However, the first quintet state ($^5A_1$) is not much above the ground state in these species (<0.5 eV). Its coupling to the porphyrin radical in Compound I-like species creates another low-lying quartet/sextet manifold that has not previously been discussed. Since this manifold may be less than 10 kcal/mol above the ground state (the B3LYP value of ~12 kcal/mol is likely to be an overestimate based on our ab initio results) it may open another channel for multistate reactivity that needs to be explored in future work. In particular, since the crossing from one quartet surface ($S_{FeO} = 1$ ferromagnetically coupled to $S_P = {}^1/_2$) to another ($S_{FeO} = 2$ antiferromagnetically coupled to $S_P = {}^1/_2$) is not spin-forbidden and since the two states differ by a d−d-orbital excitation, their SOC is expected to be efficient.

Clearly, this study cannot be all-comprehensive, especially in view of the extremely large amount of work that has been done in the field of cytochrome P450. We hope that it motivates experimentalists to continue the search for the spectroscopic signatures of the elusive Compound I intermediate of $P450_{cam}$. We believe that the combined use of QM/MM, DFT, and ab initio methods allows for a realistic modeling of the spectroscopic properties of enzyme intermediates in general, and will therefore find many future applications.

Acknowledgment. We acknowledge financial support by the Max-Planck-Gesellschaft and the German-Israeli Foundation. J.C.S. thanks the Fonds der Chemischen Industrie for a Kekulé scholarship. F.N. thanks the Deutsche Forschungsgemeinschaft for support within the priority program 1137 (Molecular

(69) Judging from the results obtained for **4** and **5**, this prediction should be viewed with some caution.

(70) This should not be confused with the spin contamination present in spin-unrestricted Hartree−Fock or DFT calculations. The mixing of different spin states is brought about by the SOC which is parametrized through the ZFS tensor in the spin-Hamiltonian treatment. Thus, this mixing represents a real physical effect and not an artifact of a computational method.

(71) (a) Schulz, C. E.; Devaney, P. W.; Winkler, H.; Debrunner, P. G.; Doan, N.; Chiang, R.; Rutter, R.; Hager, L. P. *FEBS Lett.* **1979**, *103*, 102. (b) Rutter, R.; Valentine, M.; Hendrich, M. P.; Hager, L. P.; Debrunner, P. G. *Biochemistry* **1983**, *22*, 4769.

(72) (a) Zhang, Y.; Mao, J.; Oldfield, E. *J. Am. Chem. Soc.* **2002**, *124*, 7829. (b) Liu, T. Q.; Lovell, T.; Han, W. G.; Noodleman, L. *Inorg. Chem.* **2003**, *42*, 5244. (c) Lovell, T.; Han, W. G.; Liu, T.; Noodleman, L. *J. Am. Chem. Soc.* **2002**, *124*, 5890. (d) Lovell, T.; Li, J.; Liu, T.; Case, D. A.; Noodleman, L. *J. Am. Chem. Soc.* **2001**, *123*, 12392.

(73) (a) Ghosh, P.; Bill, E.; Weyhermüller, T.; Neese, F.; Wieghardt, K. *J. Am. Chem. Soc.* **2003**, *125*, 1293. (b) Garcia Serres, R.; Grapperhaus, C. A.; Bothe, E.; Bill, E.; Weyhermüller, T.; Neese, F.; Wieghardt, K. *J. Am. Chem. Soc.* **2004**, *126*, 5138. (c) Li, M.; Bonnet, D.; Bill, E.; Neese, F.; Weyhermüller, T.; Blum, N.; Sellmann, D.; Wieghardt, K. *Inorg. Chem.* **2002**, *41*, 3444.

Magnetism). We are grateful for the constructive criticism of one reviewer.

Supporting Information Available: Details of the methods used to calculate spectral parameters. Cartesian coordinates for models **1**−**7**. The calculated optical spectrum of **2** and an analysis of the physical origin of the ZFS in the Fe(IV)O unit. Details of the coupling in **6** and **7** to the $S_{FeO} = 2$ state. This material is available free of charge via the Internet at http://pubs.acs.org.

JA0424732